# Angular momentum alignment-to-orientation conversion in the ground state of Rb atoms at room temperature

A. Mozers,* L. Busaite, D. Osite, and M. Auzinsh
*Laser Centre, University of Latvia, Rainis Boulevard 19, LV-1586 Riga, Latvia*

(Received 3 July 2020; accepted 18 September 2020; published 2 November 2020)

We investigated experimentally and theoretically angular momentum alignment-to-orientation conversion created by the joint interaction of laser radiation and an external magnetic field with atomic rubidium at room temperature. In particular, we were interested in alignment-to-orientation conversion in the atomic ground state. In the experiment the laser frequency was fixed to the hyperfine transitions of the $D_1$ line of rubidium. To simulate the measured signals we used a theoretical model that takes into account all neighboring hyperfine levels, the mixing of magnetic sublevels in an external magnetic field, the coherence properties of the exciting laser radiation, and the Doppler effect. The experiments were carried out by exciting the atoms with linearly polarized laser radiation. Two orthogonal circularly polarized laser induced fluorescence (LIF) components were detected and afterward their difference was taken. The combined LIF signals originating from the hyperfine magnetic sublevel transitions of $^{85}$Rb and $^{87}$Rb rubidium isotopes were included. The alignment-to-orientation conversion can be incontrovertibly identified in the difference signals for various laser frequencies, and a change in signal shapes can be observed when the laser power density is increased. We studied the formation of and the underlying physical processes behind the observed signals of the LIF components and their difference by performing an analysis of the influence of incoherent and coherent effects. We performed simulations of theoretical signals that showed the influence of ground-state coherent effects on the LIF difference signal.

DOI: 10.1103/PhysRevA.102.053102

## I. INTRODUCTION

Laser radiation by its very nature has a spatially anisotropic electric field distribution. First, if we neglect beam divergence, the laser beam defines a direction in space to which the vector of the electric field of the light is always perpendicular. In other words, the light electric field is always in a plane perpendicular to the beam direction. In addition, the laser radiation very often is polarized.

When such a radiation is absorbed by an ensemble of atoms, it creates an anisotropic spatial distribution of angular momentum in atoms. This anisotropy in the spatial distribution of angular momentum has the same spatial symmetry as the electric field vector of the exciting light.

When the laser beam is linearly polarized, it causes the angular momenta of the atoms in the excited state to become aligned. If the absorption is nonlinear, alignment is created in the ground state of the atoms as well. Angular momentum alignment can be imagined as a double-headed arrow. Let us set the quantization axis along the external magnetic field. If the angular momentum of the atoms is aligned along the quantization axis, the alignment is called longitudinal. In the case of longitudinal alignment the populations of magnetic sublevels with quantum number $+m_F$ and $-m_F$ are equal, but the population is different for different $|m_F|$ states. But if the angular momentum is aligned perpendicularly to the quantization axis (called transverse alignment), it means that there is a coherence created between magnetic sublevels with quantum numbers that differ by $\Delta m_F = \pm 2$ (for details see [1,2]).

In a similar way we can introduce longitudinal and transverse orientation of angular momentum. Usually orientation can be created by a circularly polarized laser excitation. In the case of orientation of the angular momentum, the spatial distribution can be represented symbolically by a single-headed arrow, and in the case of longitudinal orientation the magnetic sublevels with quantum numbers $+m_F$ and $-m_F$ in general have different populations. However, the case of transverse orientation corresponds to coherence between magnetic sublevels with values that differ by $\Delta m_F = \pm 1$ [1,2].

Changes in the fluorescence polarization, such as depolarization of laser-induced fluorescence in the magnetic field—the Hanle effect [3]—or the rotation of the plane of polarization of laser radiation that propagates in a gas of atoms [4], have a broad range of applications. For example, these effects can be used to measure the magnetic field. Other manifestations and applications of magneto-optical resonances include electromagnetically induced transparency [5], information storage in atoms [6,7], atomic clocks [8], various types of optical switches [9] and filters [10], as well as optical isolators [11].

Under some specific conditions the alignment created by excitation with a linearly polarized laser can be converted into orientation. This process is called alignment-to-orientation conversion (AOC) [2]. For this process to take place, some additional perturbation is needed, such as a magnetic field gradient [12] or anisotropic collisions [13–15].

*arturs.mozers@lu.lv

 

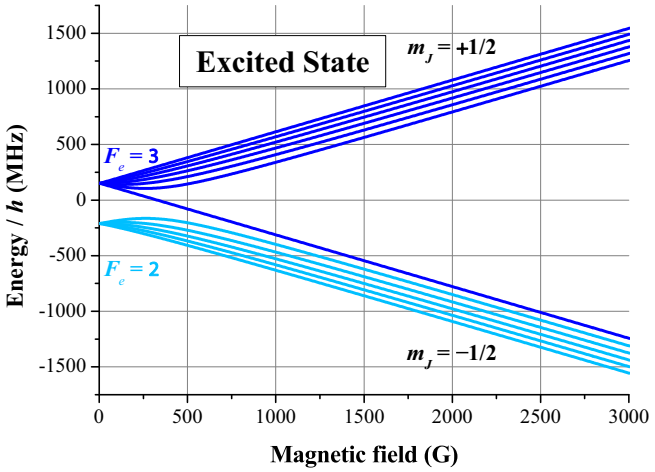


FIG. 1. Frequency shifts of the magnetic sublevels $m_F$ of the excited-state fine-structure level $5^2P_{1/2}$ as a function of magnetic field for $^{85}$Rb. Zero frequency shift corresponds the excited-state fine-structure level $5^2P_{1/2}$.

Unlike an electric field [16,17], a magnetic field alone cannot create atomic angular momentum orientation from an initially aligned ensemble, because it is an axial field that has even parity. In other words, it is symmetric under reflection in the plane perpendicular to the field direction. However, if the strength of the magnetic field interaction with an atom is comparable to the hyperfine interaction in the atom, the joint action of both interactions can cause AOC [18].

At intermediate values of the magnetic field strength the hyperfine interaction can cause a nonlinear dependence of the energies of the magnetic sublevels on the magnitude of the magnetic field—the nonlinear Zeeman or hyperfine Paschen-Back effect (see Figs. 1 and 2). If, in addition, we have exciting radiation that is linearly polarized in such a way that it contains simultaneously linear ($\pi^0$) and circular ($\sigma^{\pm}$) polarization components in the reference frame defined

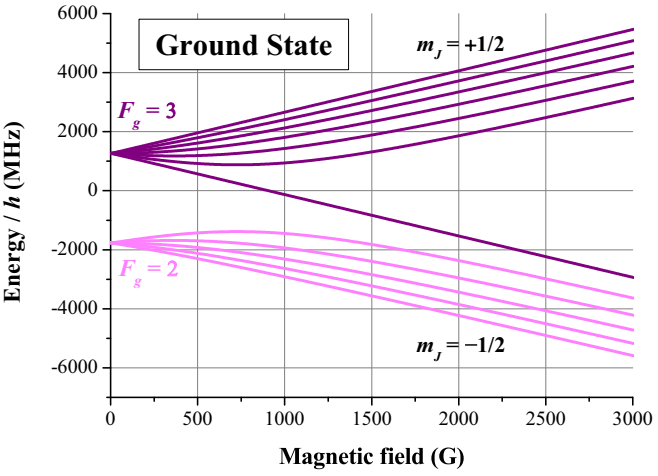


FIG. 2. Frequency shifts of the magnetic sublevels $m_F$ of the ground-state fine-structure level $5^2S_{1/2}$ as a function of magnetic field for $^{85}$Rb. Zero frequency shift corresponds to the ground-state fine-structure level $5^2S_{1/2}$.

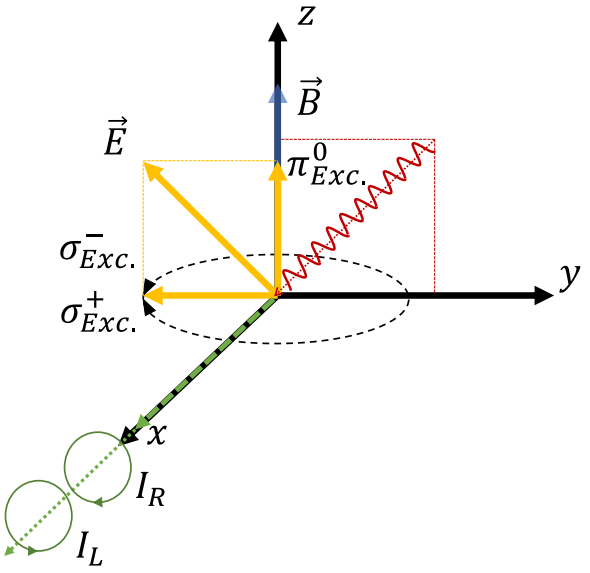


FIG. 3. Excitation and observation geometry. The linearly polarized excitation laser light $\vec{E}$ can be split into two circularly polarized excitation light components $\sigma^{\pm}_{\text{Exc}}$ and one linearly polarized excitation light component $\pi^0_{\text{Exc}}$.

by the magnetic field direction (see Fig. 3), then $\Delta m_F = 1$ coherences can be created, which leads to the breaking of the symmetry of the angular momentum spatial distribution [18] and creates the angular momentum orientation in a direction transverse to the magnetic field direction.

AOC in an external magnetic field was first studied theoretically for cadmium [19] and sodium [20], and observed experimentally in cadmium [21] and in the $D_2$ line of rubidium atoms [22]. Also the conversion in the opposite sense—conversion of an oriented state into an aligned one—is possible [23].

In the previous studies AOC caused by the joint action of an external magnetic field and the internal hyperfine interaction was studied in the excited state of rubidium atoms [18,24]. The magnetic sublevels of the excited-state angular momentum hyperfine levels in Rb atoms in an external magnetic field start to be affected by the nonlinear Zeeman effect already at moderate field strengths on the order of several tens of gauss. It should be noted that at such values of the magnetic field strength, the ground-state Zeeman effect is still close to linear.

The strongest alignment-to-orientation conversion happens at the magnetic field strength at which coherently excited magnetic sublevel pairs undergo level crossing due to nonlinear magnetic sublevel splitting [18,24]. Such level crossings do not happen in the ground state of alkali atoms. For this reason the question of AOC in the ground state is usually not analyzed. At the same time it is known (see for example [18]) that, although level crossing strongly enhances AOC signals, conversion can also happen without level crossing. The only requirement is that the excitation conditions are such that between certain magnetic sublevels coherences can be created, for example, due to the finite absorption linewidth of the atoms and the width of the spectral profile of the laser radiation.

The aim of this study is to examine AOC-creating processes in detail and to trace AOC in a particular case to the various effects that are active in the AOC—processes in the excited state, processes in the ground state, changes in the absorption probabilities caused by the magnetic sublevel scanning in the external magnetic field, and the fact that several isotopes of an atom can interact with the same laser radiation simultaneously.

Although AOC effects usually are small, especially those that are caused in the ground state of atoms, it is important to have a clear understanding of them not only out of theoretical interest, but also because of practical and fundamental applications in which they can play an important role.

The signals obtained from experiments were analyzed by a numerical theoretical model based on the optical Bloch equations (see Sec. II). We carried out experiments where two oppositely circularly polarized laser induced fluorescence (LIF) components and, afterward, their difference were observed (Sec. III). A detailed explanation of the observed experimental signals, which clearly show AOC taking place, is provided in Sec. IV.

## II. THEORETICAL MODEL

Prior to the experimental measurement, we assessed which hyperfine transitions in Rb atoms are the most suitable for detecting alignment-to-orientation conversion in the atomic ground state. To estimate the expected signal strengths and to analyze the experimental signals, we used the Liouville or optical Bloch equations (OBEs) for the density matrix $\rho$. The atomic density matrix was written in a basis defined by the whole manifold of hyperfine levels in the ground and excited states: $|\xi, F_i, m_{F_i}\rangle$, where $F_i$ refers to the quantum number of the hyperfine angular momentum in the ground ($i = g$) or the excited ($i = e$) state, $m_{F_i}$ denotes the respective magnetic quantum number, and $\xi$ represent all the other quantum numbers that are not essential for the current study.

The time evolution of the density matrix was described by the optical Bloch equations [25]

$$i\hbar\frac{\partial\rho}{\partial t} = [\hat{H}, \rho] + i\hbar\hat{R}\rho, \tag{1}$$

where $\hat{H}$ is the total Hamiltonian operator of the system and $\hat{R}$ is the relaxation operator. The full Hamiltonian can be written as $\hat{H} = \hat{H}_0 + \hat{H}_B + \hat{V}$, where $\hat{H}_0$ is the unperturbed system Hamiltonian, $\hat{H}_B$ describes the interaction with the external magnetic field, and $\hat{V} = -\hat{\mathbf{d}} \cdot \mathbf{E}(t)$ is the operator that describes the atom–laser field interaction in the electric dipole approximation. The operator includes the electric field of the exciting light $\mathbf{E}(t)$ and an electric dipole operator $\hat{\mathbf{d}}$.

The general OBEs (1) can be transformed into explicit rate equations for the Zeeman coherences within the ground ($\rho_{g_i g_j}$) and excited ($\rho_{e_i e_j}$) states by applying the rotating-wave approximation, averaging over and decorrelating from the stochastic phases of the laser radiation, and adiabatically eliminating the optical coherences [26–29]:

$$\frac{\partial\rho_{g_i g_j}}{\partial t} = \left(\Xi_{g_i e_m} + \Xi^*_{g_j e_k}\right)\sum_{e_k, e_m} d^*_{g_i e_k} d_{e_m g_j}\rho_{e_k e_m} - \sum_{e_k, g_m}\left(\Xi^*_{g_j e_k} d^*_{g_i e_k} d_{e_k g_m}\rho_{g_m g_j} + \Xi_{g_i e_k} d^*_{g_m e_k} d_{e_k g_j}\rho_{g_i g_m}\right)$$
$$- i\omega_{g_i g_j}\rho_{g_i g_j} + \sum_{e_k e_l}\Gamma^{e_k e_l}_{g_i g_j}\rho_{e_k e_l} - \gamma\rho_{g_i g_j} + \lambda\delta(g_i, g_j), \tag{2a}$$

$$\frac{\partial\rho_{e_i e_j}}{\partial t} = \left(\Xi^*_{g_m e_i} + \Xi_{g_k e_j}\right)\sum_{g_k, g_m} d_{e_i g_k} d^*_{g_m e_j}\rho_{g_k g_m} - \sum_{g_k, e_m}\left(\Xi_{g_k e_j} d_{e_i g_k} d^*_{g_k e_m}\rho_{e_m e_j} + \Xi^*_{g_k e_i} d_{e_m g_k} d^*_{g_k e_j}\rho_{e_i e_m}\right) - i\omega_{e_i e_j}\rho_{e_i e_j} - (\Gamma + \gamma)\rho_{e_i e_j}. \tag{2b}$$

Equation (2a) describes the time evolution of the populations and Zeeman coherences in the manifold of magnetic sublevels of all the hyperfine levels in the atomic ground state. The first term describes the repopulation of the ground state and the creation of Zeeman coherences due to induced transitions, while $\Xi_{g_i e_m}$ and $\Xi^*_{g_j e_k}$ represent the strength of the atom–laser field interaction. The matrix element $d_{g_i e_j} = \langle g_i|\hat{\mathbf{d}} \cdot \mathbf{e}|e_j\rangle$ is the dipole transition matrix element for transition between hyperfine magnetic sublevels $g_i$ and $e_j$ when excited by laser radiation with polarization $\mathbf{e}$. The dipole transition matrix element is calculated using the rule of scalar product for complex vectors and the Wigner-Eckart theorem [1], from which the reduced dipole matrix element $||d||$ is excluded, because it is transferred to the reduced Rabi frequency, Eq. (7). The second term denotes the changes in the ground-state Zeeman sublevel population and the creation of ground-state Zeeman coherences due to light absorption. The third term describes the influence of the external magnetic field on the ground-state Zeeman coherences, where $\omega_{g_i g_j}$ is the energy difference between magnetic sublevels $|i\rangle$ and $|j\rangle$. The fourth term describes the repopulation and transfer of excited-state coherences to the ground state due to spontaneous transitions. The transitions are closed within the hyperfine structure, so that $\sum_{e_i e_j}\Gamma^{e_i e_j}_{g_i g_j} = \Gamma$. The fifth and sixth terms in (2a) describe the transit relaxation in the ground state. The fifth term accounts for the process of thermal motion in which atoms leave the region of interaction with a spatially restricted laser beam. The rate of this process is characterized by the constant $\gamma$. It is assumed that the atomic equilibrium density matrix outside the interaction region is the unit matrix $\hat{1}$ divided by the total number of the magnetic sublevels $n_g$ in the ground-state hyperfine manifold. Therefore the repopulation rate is connected to the transit relaxation rate $\gamma$ as $\lambda = \gamma/n_g$, where $n_g$ is the total number of magnetic sublevels in the ground state. The transit relaxation rate $\gamma$ can be roughly estimated as the inverse of the average time that atoms spend

in the laser beam when they are traversing it due to thermal motion.

Similarly to Eq. (2a), in Eq. (2b) the first term denotes the changes in the excited-state density matrix caused by light absorption, the second term describes induced transitions to the ground state, the third stands for the influence of the external magnetic field on the excited-state Zeeman coherences, where $\omega_{e_i e_j}$ is the splitting of the excited-state Zeeman sublevels. Finally, the fourth term describes the combined rate of spontaneous decay and transit relaxation (atoms are leaving the region where they interact with laser radiation due to thermal motion) of the excited state.

The atom–laser radiation interaction strength $\Xi_{g_i e_j}$, used in (2), is expressed as

$$\Xi_{g_i e_j} = \frac{\Omega_R^2}{\frac{\Gamma+\gamma+\Delta\omega}{2} + i\left(\bar{\omega} - \mathbf{k}_{\bar{\omega}} \cdot \mathbf{v} + \omega_{g_i e_j}\right)}, \tag{3}$$

where $\Omega_R$ is the reduced Rabi frequency, $\Omega_R^2$ being proportional to the laser power density. The term $\Delta\omega$ represents the finite spectral width of the exciting radiation, $\bar{\omega}$ is the central frequency of the exciting radiation, $\mathbf{k}_{\bar{\omega}}$ is the wave vector of exciting radiation, and $\mathbf{k}_{\bar{\omega}} \cdot \mathbf{v} = 2\pi\Delta_D$ is the Doppler shift experienced by an atom moving with velocity $\mathbf{v}$.

Since the experiments were conducted at continuous wave excitation conditions, we were interested in the stationary solution of Eqs. (2),

$$\frac{\partial \rho_{g_i g_j}}{\partial t} = \frac{\partial \rho_{e_i e_j}}{\partial t} = 0, \tag{4}$$

reducing the differential Eqs. (2) to a system of linear equations. The solution of the system yields density matrices for the ground and excited states.

The observed fluorescence intensity $I_{\text{ob}}$ of polarization $\mathbf{e}_{\text{ob}}$ then was calculated from the excited-state density matrix elements as

$$I_{\text{ob}}(\mathbf{e}_{\text{ob}}) = \tilde{I}_0 \sum_{g_i, e_j, e_k} d^{*(\text{ob})}_{g_i e_j} d^{(\text{ob})}_{e_k g_i} \rho_{e_j e_k}, \tag{5}$$

where $d^{(\text{ob})}_{e_k g_i} = \langle e_k | \hat{\mathbf{d}} \cdot \mathbf{e}_{\text{ob}} | g_i \rangle$ are the dipole transition matrix elements for the radiation with specific polarization ($\mathbf{e}_{\text{ob}}$) observed in a chosen direction. $\tilde{I}_0$ is the constant of proportionality.

The thermal motion of the atoms was accounted for by signal averaging over the thermal velocity distribution of atoms. This averaging was performed by solving Eqs. (2) for each velocity group, accounting for the relative probability of an atom to have this velocity and averaging the fluorescence intensity (5) over this distribution.

To simulate the expected signals and to fit the experimental results, we estimated the values of several parameters to first approximation.

The transit relaxation rate was estimated from the mean thermal velocity $v_{th}$ of the atoms projected onto the plane perpendicular to the laser beam and from the laser beam diameter $d$:

$$\gamma = \frac{v_{th}}{d}. \tag{6}$$

For $d = 1400$ $\mu$m and $T = 293$ K we estimated $\gamma = 2\pi \times (0.019$ MHz).

The reduced Rabi frequency was estimated as

$$\Omega_R = k_R \frac{||d|| \times |\varepsilon|}{\hbar} = k_R \frac{||d||}{\hbar} \sqrt{\frac{2I}{\epsilon_0 n c}}, \tag{7}$$

where $k_R$ is a dimensionless fitting parameter, $||d|| = 4.231 e a_0$ [1] is the reduced dipole matrix element for the $D_1$ transition, $e$ is the electron charge, and $a_0$ is the Bohr radius [30]. The term $I$ represents the power density (directly related to the amplitude of the electric field $|\varepsilon|$), $\epsilon_0$ is the electric constant, $n$ is the refractive index, and $c$ is the speed of light.

In practice, the power density $I$ is not constant across the laser beam, so that the estimation of the parameter $k_R$ is not straightforward. The theoretical model used a constant value for the power density instead of the actual power distribution. As the power density is increased, $\Omega_R$ cannot be related to the square root of the power density $I$ by the same constant $k_R$ as for the lower power densities [29,31], if one merely assumes that the laser power density distribution within the beam is Gaussian.

This leads to a more complex relationship between $I$ and $\Omega_R$, which has a simple explanation. Our experiment was performed in the regime of nonlinear absorption, which leads to strong depletion of the ground-state population for large laser power densities. For low laser power density, the ground-state population is only slightly changed, even at the center of the beam, where the light is most intense. However, when the laser power is increased, the atoms in the center of the beam are more actively excited, leaving a diminished ground-state population in the center of the beam. When the laser power density is increased even more, the region of population depletion expands to the "wings" of the Gaussian power density distribution.

Due to this spatially dependent population depletion, the main contribution to the signal for weaker laser radiation comes from the central parts of the laser beam where the power density is the highest, and the theoretical proportionality of $\Omega_R$ to the square root of power density continues to hold. However, for stronger laser radiation power density, the peripheral parts of the laser beam, where power density is lower, start to play a larger role in the absorption process, because the ground-state population there is more significant than at the center of the beam. Therefore, when increasing the laser power density, the different parts of the laser beam play a dominant part in the absorption process, which should be related to the Rabi frequency $\Omega_R$ in the theoretical model. We accounted for this effect by adjusting the value of the coefficient $k_R$ in the theoretical model to achieve better correspondence between the experimental measurements and theoretical calculations.

By finding the best agreement between theoretical and experimental signals an appropriate estimate of the spectral width used in the theoretical model was found to be $\Delta\omega = 2\pi \times (2$ MHz), which is close to the value given by the manufacturer of the laser.

## III. EXPERIMENT

The experiments were performed on atomic rubidium vapor at room temperature. The cylindrical (diameter 25 mm,

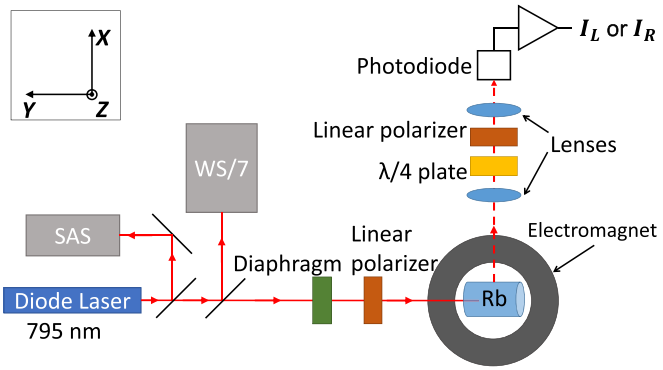


FIG. 4. Side view of the experimental setup. The beam enters the coils at an angle of 45° with respect to the $y$ axis in the $yz$ plane (axes shown in the inset).

length 25 mm) Pyrex atomic vapor cell with optical quality windows contained rubidium isotopes in their natural abundance. The atoms were excited with linearly polarized light with its polarization vector **E** in the $y$-$z$ plane and making a $\pi/4$ angle with respect to the quantization axis $z$ defined by the external magnetic field **B** as shown in Fig. 3. The two circularly polarized laser induced fluorescence (LIF) components $I_L$ and $I_R$ were observed along the $x$ direction. The LIF passed through a pair of convex lenses while $I_L$ or $I_R$ were selected by changing the relative angle between the fast axis of a zero-order quarter-wave plate and the polarization axis of a linear polarizer. These optical elements were aligned in a lens tube while the linear polarizer was rotated by means of a rotation mount.

A tuneable, grating-stabilized, external-cavity, single-mode diode laser DL 100, produced by Toptica AG, with a wavelength of 794.98 nm ($D_1$ line of Rb) and a typical linewidth of a few MHz, was used in all of the experiments. During the experiments the laser frequency was fixed to a saturation absorption spectrum (SAS) signal coming from another atomic rubidium vapor cell, which was placed in a three-layer $\mu$-metal shield. A dedicated feedback controller (DigiLock by Toptica AG) managed the laser's temperature, current, and piezo scan controllers to lock the laser to a particular peak of the SAS, i.e., to a particular hyperfine transition.

Figure 4 shows a schematic of the experimental setup. The magnetic field was applied using an electromagnet with an iron core with a diameter of 10.0 cm. The separation between the surfaces of the poles was 4.3 cm. The inhomogeneity of the field in the center of the poles was estimated to be no more than 0.027% by a finite-element electromagnetic field solver, based on the geometry of the magnet. The current for the electromagnet was supplied by a bipolar power supply, and the symmetrical triangular current scan was generated by a function generator. The frequency of the magnetic field scan was 2.00 mHz with a maximum scan amplitude resulting in a magnetic field range from −3100 to +3100 G.

The elliptical beam profile that emerged from the laser diode was corrected with a diaphragm. Using a beam profiler, the beam diameter was measured to be 1400 $\mu$m at the full width at half maximum (FWHM) of the Gaussian fit. The laser power was adjusted using a half-wave Fresnel rhomb retarder followed by a linear polarizer. In this way, the laser power values could be varied from 10 $\mu$W to 600 $\mu$W, which translates into laser power densities from 0.36 mW/cm$^2$ to 28.6 mW/cm$^2$. The LIF was detected with a photodiode (Thorlabs SM1PD1A) which was placed at the end of and fixed into the observation lens tube. The LIF from each circularly polarized component was detected independently, i.e., successively one at a time. The signal from the photodiode was amplified by a transimpedance amplifier with a gain of $10^6$, followed by a voltage amplifier with a gain of $10^4$. Every scan was acquired with an Agilent DSO5014A digital oscilloscope and transferred to a PC with a minimum of 16 scans in total for each component.

The experimental signals of each circular LIF component were averaged over multiple scans. To eliminate any residual asymmetry in the signal, the scans were averaged over the negative and positive values of the magnetic field. When comparing the experimental signals to theory, the constant background was subtracted before the signals were normalized to the maximum of each component. The background was measured by blocking the laser beam and recording the signal from the photodiode. During data processing we allowed the background value to vary for different laser power densities in order to achieve a better agreement between the experiment and the theory, but the variation of the background value never exceeded 3%, which is within the measurement error of the measured background value. As the LIF component signals were relatively large in comparison to their difference and circularity signals, a Savitzky-Golay smoothing filter [32] was applied to the LIF difference signals.

## IV. RESULTS AND DISCUSSION

Let us start with the analysis of the general structure of the observed signals. We will show only one of the components ($I_L$) in this paper as an example, since the differences in the two oppositely circularly polarized LIF components are small and can be barely seen when the two observed circularly polarized LIF components are depicted side by side. Figure 5 shows a typical result for a measurement of a single circularly polarized LIF component when the laser frequency was locked to the $F_g = 2 \rightarrow F_e = 2$ transition of the $^{85}$Rb. At zero magnetic field an initial relative minimum of the LIF signal can be observed. The increase of the magnetic field lifts the degeneracy and the LIF signal rises because of other atoms with different velocity coming into resonance. The LIF signal starts to fall after approximately 250 G. The diminishing of the signal has the same underlying mechanism as the increase in signal working in the opposite sense: the nonlinear Zeeman effect both for the ground and excited state leads to a decrease in the number of atoms that interact with the laser light. A pronounced feature can be seen at approximately 1500 G (and another at 2800 G): an increase in the LIF signal. This increase is caused by magnetic sublevels coming back into resonance with the excitation laser radiation. In particular, one can deduce exactly which magnetic sublevels are interacting with the laser field from Fig. 6. This figure shows the dependence of the energy difference $\Delta\nu$ between pairs of magnetic sublevels on the external magnetic field. When $\Delta\nu$ is equal to 0, the energy difference between pairs of magnetic sublevels coincides

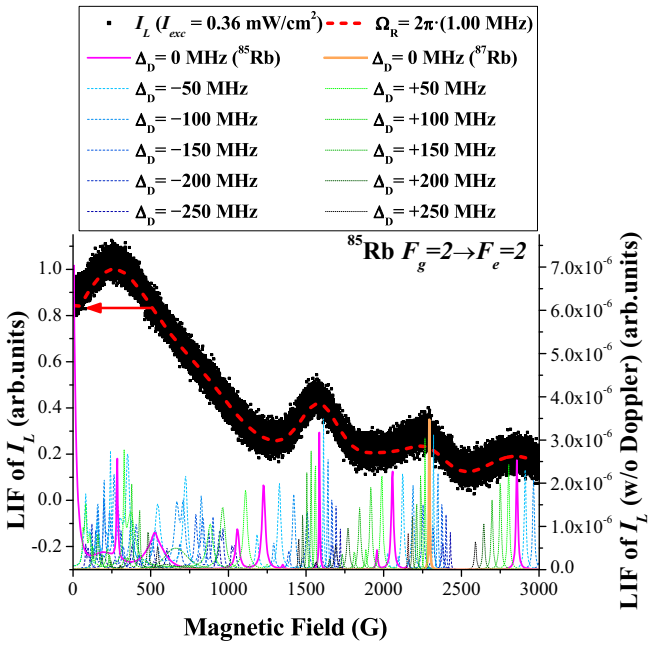


FIG. 5. LIF of a single circularly polarized light component ($I_L$). Black dots: experimental data; red dashed curve: theoretical data (left axis); colored lines: theoretical data without averaging over the Doppler profile (right axis). Magenta solid curve (dark gray): central velocity group of $^{85}$Rb; orange curve (light gray): central velocity group of $^{87}$Rb; blue short-dashed curves: negative velocity shift; green short-dotted curves: positive velocity shift.

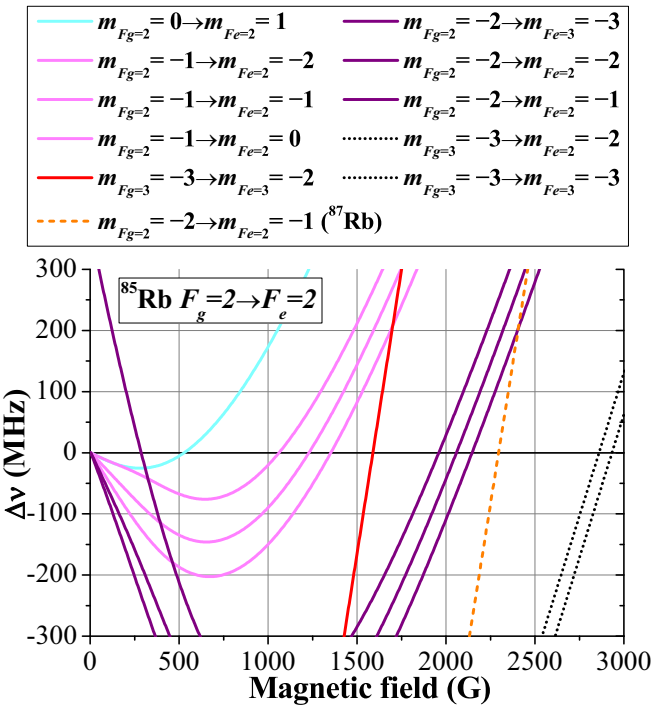


FIG. 6. The colored lines represent the dependence of the energy difference between various pairs of magnetic sublevels on magnetic field. $\Delta\nu = 0$ corresponds to laser frequency equal to the $F_g = 2 \rightarrow F_e = 2$ hyperfine transition of the $^{85}$Rb. (Only pairs crossing $\Delta\nu = 0$ are shown.)

with the laser frequency. Thus it can be easily deduced that the pair of magnetic sublevels that corresponds to the increase in LIF at 1500 G is $m_{F_g=3} = -3 \rightarrow m_{F_e=3} = -2$.

Usually magnetic sublevels from only one isotope are considered in theoretical simulations. For a complete understanding of the shapes of these signals one has to take into account both isotopes, as the magnetic field is large enough to bring the magnetic sublevels of the $^{87}$Rb hyperfine levels into resonance. In order to combine the LIF signals from both isotopes, the signals were weighted according to the difference in isotope abundance and line strength [1].

The width of these nonzero field structures in the observed signal can be attributed to the fact that the interacting atoms are in thermal motion, and so the Doppler effect plays a large role in the formation of the line shapes. The solid, short-dashed, and short-dotted curves near the bottom of Fig. 5 are the result of the LIF signal simulations, where the averaging over the Doppler profile was omitted and a single velocity group was selected from the Doppler profile. Now the width of the shapes in the experimental data as well as in the simulated red dashed curve in Fig. 5 can be interpreted as LIF coming from different velocity groups. The width of the narrow peaks appearing in the simulated LIF curves for single velocity groups is related to the width that arises from the combined action of the natural linewidth and excitation laser linewidth. The different relative amplitudes of these peaks in the LIF signals from different velocity groups are related to transition probabilities between magnetic sublevels; i.e., when an external magnetic field is applied, the wave functions of magnetic sublevels mix, and their transition probabilities change [33]. The summation over all of these LIF curves from different velocity groups (Doppler components) would yield the complete simulated LIF curve (Fig. 5, dashed red). As was shown in [34] the summation over all the velocity groups is crucial for the explanation of the observed signals.

A rather counterintuitive feature can be noticed at approximately 1250 G. The zero-velocity group LIF curve [Fig. 5, $\Delta_D = 0$ MHz, magenta (dark gray) solid] shows an increase in the signal, and in Fig. 6 magnetic sublevels $m_{F_g=2} = -1 \rightarrow m_{F_e=2} = -1$ come into resonance with the laser. However, the averaging over the Doppler profile produces a minimum in the LIF signal. To understand the cause of such a peculiar feature in the observed signal, we show LIF from several Doppler components (velocity groups) in Fig. 5 and the energy difference $\Delta\nu$ between pairs of magnetic sublevels in Fig. 6. For a peak to appear in the observed signal the shift in transition frequency between two magnetic sublevels (change in $\Delta\nu$) should be larger than the change in the absolute value of the applied magnetic field (change in **B**). When a rather large change in **B** is necessary to achieve the same change in $\Delta\nu$, the Doppler components get spread out more and as a result the overall signal is flattened, which leads to a relative minimum in the observed signal.

We performed an analogous examination of all measured circularly polarized LIF signals for different exciting laser frequencies and power densities. All experimentally obtained signals were fitted to simulated curves. Figure 7 shows all of the Rabi frequency values (squared) obtained from the data fitting procedure vs laser power density. The different colors

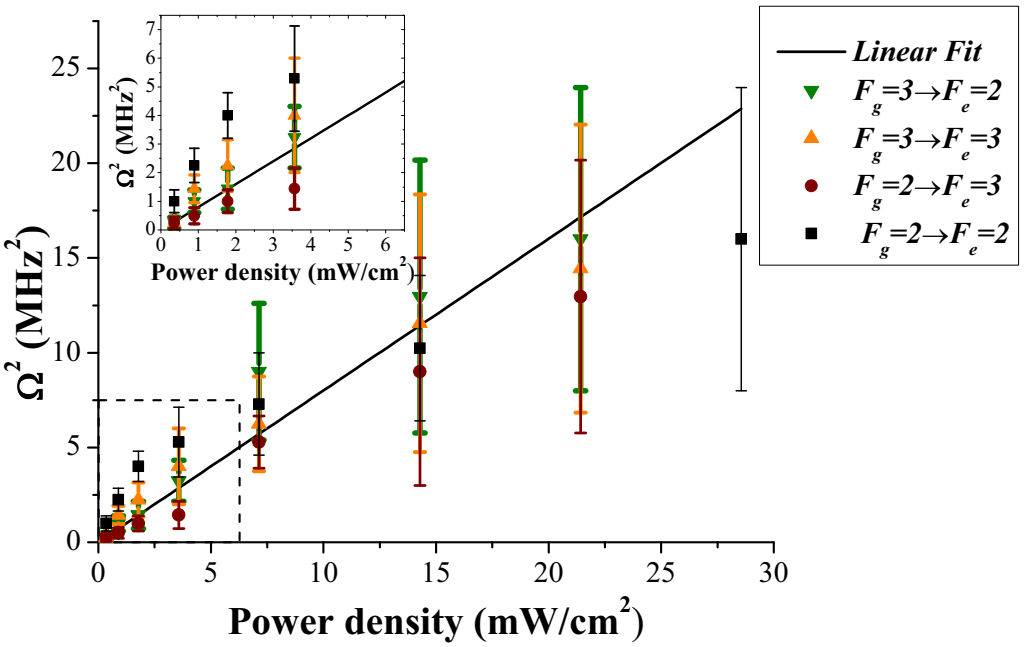


FIG. 7. Dependence of the Rabi frequency squared $\Omega_R^2$ on the laser power density $I$ together with a linear fit for all the fixed laser frequencies used in the experiment (colored data points).

in Fig. 7 correspond to different laser frequencies. The data points within the margins of error are in good agreement with a linear fit based on Eq. (7). We allowed the fitting parameter $k_R$ to vary in order to achieve better agreement between the experiment and the theoretical curves, which led to a symmetric distribution of data points in Fig. 7. Nevertheless, upon closer examination the data points show a tendency to fall below the linear fit at laser power densities above 20 mW/cm$^2$. This discrepancy is due to the fact that the theoretical model does not take into account the spatial distribution of the exciting optical field. The influence of different laser power density values at different spatial positions on the fluorescence signal, which causes the atoms to interact differently with the laser beam, has been studied in [35].

The dependence of the LIF signal on laser detuning was analyzed in terms of the difference between the two observed LIF components defined as $I_L - I_R$. We show the difference signals as they depend only on the transverse orientation of the angular momentum. The other measure of orientation, circularity $(I_L - I_R)/(I_L + I_R)$, has almost the same shape. However, it depends not only on the transverse orientation, but is slightly influenced by the angular momentum alignment as well [2].

Figure 8 shows the dependence of $I_L - I_R$ on the external magnetic field for different laser frequencies. As the laser frequency decreases [from (a) to (d) in Fig. 8], a change in line shapes can be observed. The difference signal when the laser frequency was fixed to the $F_g = 2 \rightarrow F_e = 3$ transition of the $^{85}$Rb changes from slightly positively circularly polarized light (from $\approx +0.5\%$ when converted to circularity values) to slightly negatively circularly polarized light ($\approx -0.5\%$). This indicates that the transverse orientation of the angular momentum of the ensemble of atoms also changes from slightly positive values to slightly negative values. In contrast, when the laser frequency was fixed to other hyperfine transitions, the sign of the difference signal did not change depending on the magnetic field. The largest circularity value of $\approx$4% was observed when the laser frequency was set to the $F_g = 2 \rightarrow F_e = 2$ transition of the $^{85}$Rb.

For the purpose of this study it is important to examine how the difference signal for the two circularly polarized

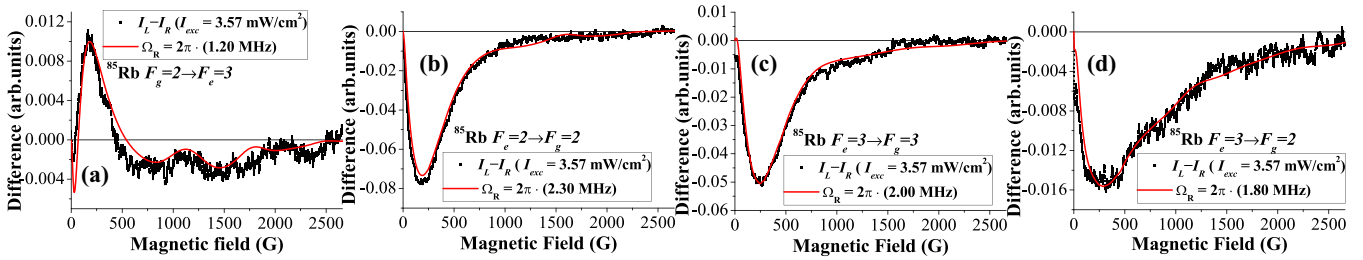


FIG. 8. The dependence of the difference between the two LIF components on the hyperfine transitions to which the laser frequency was fixed. The laser frequency was fixed to (a) $F_g = 2 \rightarrow F_e = 3$, (b) $F_g = 2 \rightarrow F_e = 2$, (c) $F_g = 3 \rightarrow F_e = 3$, (d) $F_g = 3 \rightarrow F_e = 2$ hyperfine transition of $^{85}$Rb. (a)–(d) laser frequencies are in descending order.

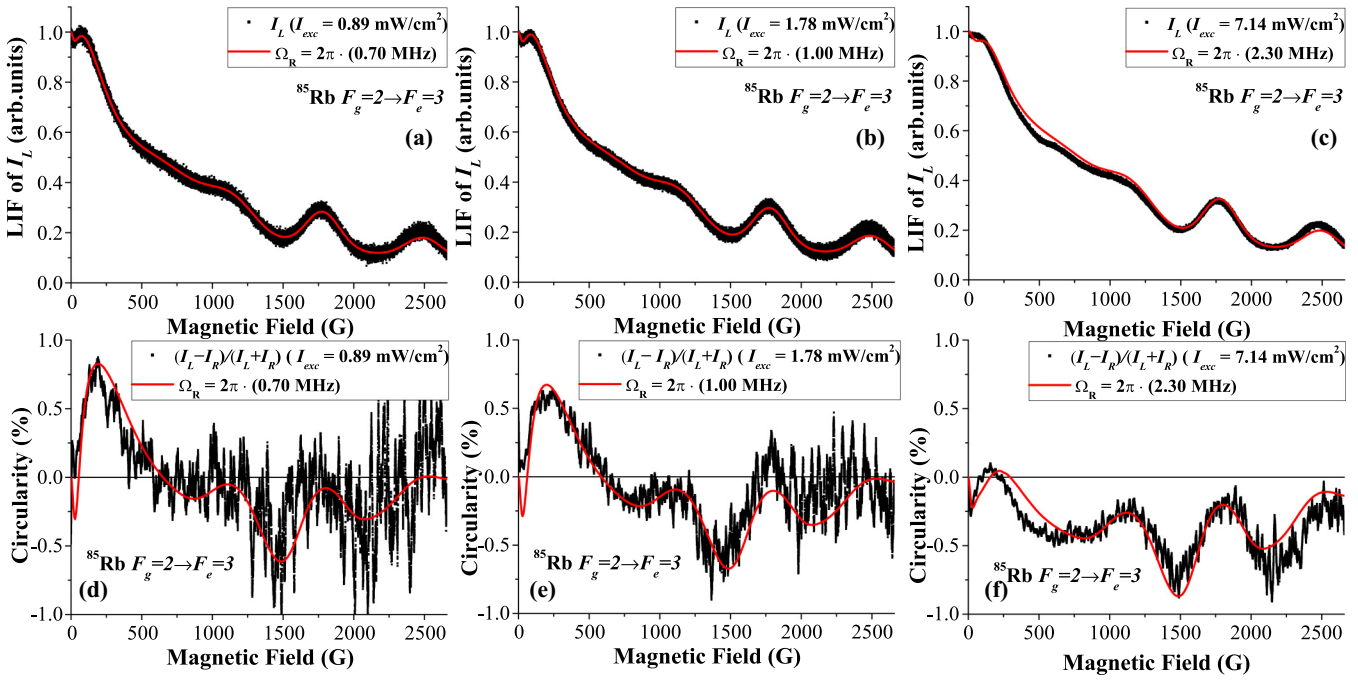


FIG. 9. The first row (a)–(c) shows the signal of a single circularly polarized LIF component $I_L$ as a function of laser power density. The second row (d)–(f) shows the corresponding circularity dependence on laser power density for the case when the laser frequency was fixed to the $F_g = 2 \rightarrow F_e = 3$ hyperfine transition of $^{85}$Rb. Black dots: experimental data; red curve: theoretical calculation.

fluorescence components (which in the chosen geometry of excitation-observation is directly proportional to the transverse orientation of the angular momentum) depends on the power density of the excitation radiation. This dependence serves as one of the indicators that helps to separate the effects of the atomic excited state, which are present even in the linear absorption region, from the ground-state effects that are intrinsically nonlinear with respect to the light intensity and do not manifest themselves at weak excitation laser power density.

Figure 9 shows the signal dependence on laser power density for the case when the laser frequency was fixed to the $F_g = 2 \rightarrow F_e = 3$ transition of the $^{85}$Rb. As the laser power is being increased, the aforementioned change of the sign of circularity disappears for laser power densities greater than 1.78 mW/cm$^2$; i.e., for all magnetic field values the circularity stays negative. In order to understand the root cause of the circularity line shapes, theoretical simulations that omit the averaging over the Doppler profile were carried out for various velocity groups of the Doppler profile (Fig. 10). The pronounced peak (structure) seen in Fig. 9(d) at approximately 1500 G would appear to be connected with magnetic sublevels that come into resonance with the laser light, but the LIF component signals in Figs. 9(a)–9(c) clearly show a minimum at 1500 G. The origin of this nonzero circularity can be understood by looking at Fig. 10: as different velocity groups come into resonance some shift the transverse orientation of the angular momentum in the positive direction and some in the negative. When the signals from all of these contributing velocity groups are combined, only the ones that were not compensated by other velocity groups contribute to the observed circularity signal. The arbitrary units in both vertical axes in Fig. 10 are directly comparable. The right vertical axis corresponds to the LIF signals from different velocity groups. The signals from all the velocity groups, of which only a few are shown in Fig. 10, are summed to obtain the red, dashed curve, which corresponds to the left vertical axis.

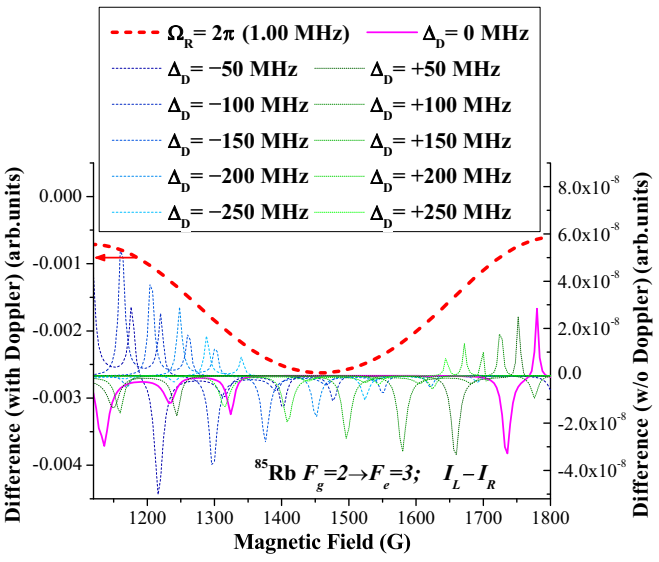


FIG. 10. Red dashed curve (left axis): theoretical data of the difference between two circularly polarized light components ($I_L - I_R$) with averaging over the Doppler profile. Colored curves (right axis): theoretical data of the difference between two circularly polarized light components without averaging over the Doppler profile. Different colors represent various velocity groups from the Doppler profile. Magenta solid curve (dark gray): central velocity group; blue short-dashed curves: negative velocity shift; green short-dotted curves: positive velocity shift.

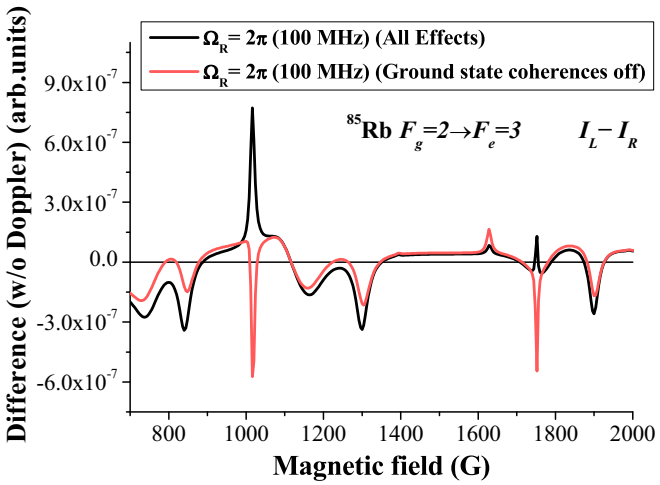


FIG. 11. $I_L - I_R$ dependence on the magnetic field from the central velocity group; averaging over the Doppler profile is omitted. Red curve: theoretical data from $^{85}$Rb with Rabi frequency 100 MHz with large $\gamma_{\text{nondiagonal}}$; black curve: theoretical data from $^{85}$Rb with Rabi frequency 100 MHz with normal $\gamma_{\text{nondiagonal}}$.

The transverse angular momentum AOC is a coherent effect. A coherent superposition of atomic states is the basis for many interesting and useful effects in atomic and molecular physics: the linear and nonlinear Hanle effect [36], electromagnetically induced transparency (EIT) [37], stimulated Raman adiabatic passage (STIRAP) [38], "slow" and "superluminal" light [39], coherent population trapping (CPT) [40], and lasing without inversion [41] are just some of these effects. Several of them are exclusively related to coherences in the excited state of atoms and several in the atomic ground state.

With this in mind we wanted to distinguish between the ground-state coherent effects and the excited-state coherent effects that contribute to the observed AOC signal. At low Rabi frequencies the effect of ground-state coherence transfer was minute, and because the underlying causes for the signal shapes can be better understood by analyzing the LIF signals that come from separate velocity groups (omitting the averaging over the Doppler profile), we show the simulated curves in Fig. 11 for the central velocity group (with respect to the exciting laser frequency) with large Rabi frequency.

With the aim of determining which features in the signal are caused by ground-state coherent effects, we set the nondiagonal density matrix elements [in Eq. (2a)] to zero. We did this by increasing the relaxation rate $\gamma_{\text{nondiagonal}}$ of only these elements with the ratio of $\gamma_{\text{nondiagonal}}/\gamma_{\text{diagonal}} = 10^9$ with respect to the $\gamma_{\text{diagonal}}$, which is the normal transit relaxation rate experienced by diagonal elements. This allowed us to observe the influence of the transfer of coherence from the ground state to the excited state. Figure 11 shows the comparison of the two cases of simulated LIF signals from the central velocity group. The red curve (in Fig. 11) corresponds to the case when the ground-state coherent effects were set to zero whereas the black curve shows the case when all the elements in the density matrix experience normal relaxation.

As can be seen from the differences in the two curves (Fig. 11); some features, e.g., at approximately 1300 G, persist in both curves virtually unchanged, but other features experience a dramatic change. For example, the features at 1000 G and 1750 G changed dramatically, which indicates that these features are directly connected to the ground-state coherent effects. Both features show a change in the direction of angular momentum orientation when the ground-state coherences were set to zero $I_L < I_R$, while the black curve shows the signal to be $I_L > I_R$ when the parameters for all effects were set to normal values. When the averaging over the Doppler profile is included, these features become less pronounced as the signals from different velocity groups compensate each other, causing the overall signal to approach zero (much like in the analysis of Fig. 10). This is partially verified by experimentally observed signals: the features at 1000 G and 1750 G [see Fig. 9(f)] also tend toward an increase in the $I_L - I_R$ signal.

## V. CONCLUSION

When the coherent effects in the manifold of atomic angular momentum magnetic sublevels, induced by the interaction of atoms with laser radiation, are conceptually discussed, very often the preponderance of attention is paid to the creation of coherent superpositions of these sublevels due to two factors: first, excitation light polarization components capable of exciting coherently these sublevels are considered and, second, transition probabilities determined by the transition dipole moments between angular momentum states are accounted for [1].

In this paper we analyze in detail and show that on top of these effects a very important role in this process is played by the magnetic scanning of the magnetic sublevels in the external magnetic field. In the Paschen-Back regime two effects are important: first, nonlinear magnetic sublevel splitting that can lead to symmetry breaking of the spatial distribution of angular momentum—the alignment-to-orientation conversion—and, second, changes in the transition probabilities due to magnetic sublevel mixing in the magnetic field.

Another very important aspect of the analysis of laser light–atom interaction is the necessity of a clear separation of incoherent (related to the populations distribution of magnetic sublevels) and coherent (determined by well-defined phase relations of magnetic sublevel wave functions) contributions to the observed signals.

In this paper we have shown that, for example, in the Rb atoms used in this study, at different values of the magnetic field strength, not only different hyperfine transitions of a specific isotope of an atom come into resonance with laser radiation, but the same laser radiation at different values of the magnetic field strength can excite hyperfine transitions in different isotopes of rubidium atoms. This effect appears because of magnetic sublevel scanning and primarily is an incoherent effect (see Fig. 5 the subsequent analysis).

Finally, based on the comparison of signals obtained from a numerical model in which we are able to "switch-off" and "switch-on" different relaxation processes, we managed to show that specific features in the observed signals are determined by the alignment-to-orientation conversion in the atomic ground state (see Figs. 9 and 11 and the analysis there). We believe that alignment-to-orientation conversion

in the ground state of atoms has not been identified before. The clear understanding of the presence of these effects is important for applications as well as for fundamental research using table-top atomic physics experiments, such as in the search for a permanent electric dipole moment (EDM) of an electron. In EDM experiments [42,43] performed with atoms and polar diatomic molecules [44] even a very small misalignment between applied external magnetic and electric fields can complicate the interpretation of the results.


## ACKNOWLEDGMENTS

A.M. acknowledges support from PostDoc Latvia Grant No. 1.1.1.2/16/117 "Experimental and theoretical signals of ground-state angular momentum alignment-to-orientation conversion by the influence of laser radiation and external magnetic field in atomic alkali metal vapour." The authors are thankful to Dr. L. Kalvans for discussions and advice with LIF signal simulations and Dr. J. Smits for estimation of experimental parameters.



[1] M. Auzinsh, D. Budker, and S. Rochester, *Optically Polarized Atoms: Understanding Light-Atom Interactions* (Oxford University Press, New York, 2010).

[2] M. Auzinsh and R. Ferber, *Optical Polarization of Molecules*, Cambridge Monographs on Atomic, Molecular, and Chemical Physics (Cambridge University Press, Cambridge, UK, 2005).

[3] G. Moruzzi and F. Strumia (eds.), *The Hanle Effect and Level-Crossing Spectroscopy* (Springer US, Boston, MA, 1991).

[4] D. Budker, W. Gawlik, D. F. Kimball, S. M. Rochester, V. V. Yashchuk, and A. Weis, Resonant nonlinear magneto-optical effects in atoms, Rev. Mod. Phys. **74**, 1153 (2002).

[5] S. E. Harris, Electromagnetically induced transparency, Phys. Today **50**(7), 36 (1997).

[6] D. F. Phillips, A. Fleischhauer, A. Mair, R. L. Walsworth, and M. D. Lukin, Storage of Light in Atomic Vapor, Phys. Rev. Lett. **86**, 783 (2001).

[7] C. Liu, Z. Dutton, and C. H. Behroozi, Observation of coherent optical information storage in an atomic medium using halted light pulses, Nature (London) **409**, 490 (2001).

[8] S. Knappe, P. D. D. Schwindt, V. Shah, L. Hollberg, J. Kitching, L. Liew, and J. Moreland, A chip-scale atomic clock based on $^{87}$Rb with improved frequency stability, Opt. Express **13**, 1249 (2005).

[9] P. Yeh, Dispersive magnetooptic filters, Appl. Opt. **21**, 2069 (1982).

[10] A. Cerè, V. Parigi, M. Abad, F. Wolfgramm, A. Predojević, and M. W. Mitchell, Narrowband tunable filter based on velocity-selective optical pumping in an atomic vapor, Opt. Lett. **34**, 1012 (2009).

[11] L. Weller, K. Kleinbach, M. Zentile, S. Knappe, I. Hughes, and C. Adams, Optical isolator using an atomic vapor in the hyperfine Paschen-Back regime., Opt. Lett. **37**, 3405 (2012).

[12] U. Fano, Precession equation of a spinning particle in nonuniform fields, Phys. Rev. **133**, B828 (1964).

[13] M. Lombardi, Note sur la possibilité d'orienter un atome par super-position de deux interactions séparément non orientantes en particulier par alignement électronique et relaxation anisotrope, C.R. Acad. Sci. Paris, Ser. B **265**, 191 (1967).

[14] V. Rebane, Depolarization of resonance fluorescence during anisotropic collisions, Opt. Spectrosc. (USSR) **24**, 163 (1968).

[15] T. Manabe, T. Yabuzaki, and T. Ogawa, Observation of Collisional Transfer from Alignment to Orientation of Atoms Excited by a Single-Mode Laser, Phys. Rev. Lett. **46**, 637 (1981).

[16] M. Lombardi, Création d'orientation par combinaison de deux alignements alignement et orientation des niveaux excités d'une décharge haute fréquence, J. Phys. France **30**, 631 (1969).

[17] M. Auzinsh, K. Blushs, R. Ferber, F. Gahbauer, A. Jarmola, and M. Tamanis, Electric-Field-Induced Symmetry Breaking of Angular Momentum Distribution in Atoms, Phys. Rev. Lett. **97**, 043002 (2006).

[18] J. Alnis and M. Auzinsh, Angular-momentum spatial distribution symmetry breaking in Rb by an external magnetic field, Phys. Rev. A **63**, 023407 (2001).

[19] J. C. Lehmann, Étude de l'influence de la structure hyperfine du niveau excité sur l'obtention d'une orientation nucléaire par pompage optique, J. Phys. France **25**, 809 (1964).

[20] W. E. Baylis, Optical-pumping effects in level-crossing measurements, Phys. Lett. A **26**, 414 (1968).

[21] J. C. Lehmann, Nuclear orientation of Cadmium$^{111}$ by optical pumping with the resonance line $5^1S_0 - 5^1P_1$, Phys. Rev. **178**, 153 (1969).

[22] M. Krainska-Miszczak, Alignment and orientation by optical pumping with pi polarised light, J. Phys. B **12**, 555 (1979).

[23] H. Brändle, L. Grenacs, J. Lang, L. P. Roesch, V. L. Telegdi, P. Truttmann, A. Weiss, and A. Zehnder, Measurement of the Correlation between Alignment and Electron Momentum in $^{12}\mathrm{B} \rightarrow {}^{12}\mathrm{C}$(g.s.) Decay by a Novel Technique: Another Search for Second-Class Currents, Phys. Rev. Lett. **40**, 306 (1978).

[24] M. Auzinsh, A. Berzins, R. Ferber, F. Gahbauer, L. Kalvans, A. Mozers, and A. Spiss, Alignment-to-orientation conversion in a magnetic field at nonlinear excitation of the $D_2$ line of rubidium: Experiment and theory, Phys. Rev. A **91**, 053418 (2015).

[25] S. Stenholm, *Foundations of Laser Spectroscopy* (Dover Publications, Inc., Mineoloa, New York, 2005).

[26] K. Blushs and M. Auzinsh, Validity of rate equations for Zeeman coherences for analysis of nonlinear interaction of atoms with broadband laser radiation, Phys. Rev. A **69**, 063806 (2004).

[27] M. Auzinsh, R. Ferber, F. Gahbauer, A. Jarmola, and L. Kalvans, Nonlinear magneto-optical resonances at $D_1$ excitation of $^{85}$Rb and $^{87}$Rb for partially resolved hyperfine $F$ levels, Phys. Rev. A **79**, 053404 (2009).

[28] M. Auzinsh, A. Berzins, R. Ferber, F. Gahbauer, L. Kalvans, A. Mozers, and A. Spiss, Dependence of the shapes of nonzero-field level-crossing signals in rubidium atoms on the laser frequency and power density, Phys. Rev. A **87**, 033412 (2013).

[29] M. Auzinsh, A. Berzins, R. Ferber, F. Gahbauer, U. Kalnins, L. Kalvans, R. Rundans, and D. Sarkisyan, Relaxation mech-

anisms affecting magneto-optical resonances in an extremely thin cell: Experiment and theory for the cesium $D_1$ line, Phys. Rev. A **91**, 023410 (2015).

[30] M. Auzinsh, D. Budker, and S. M. Rochester, Light-induced polarization effects in atoms with partially resolved hyperfine structure and applications to absorption, fluorescence, and nonlinear magneto-optical rotation, Phys. Rev. A **80**, 053406 (2009).

[31] M. Auzinsh, R. Ferber, I. Fescenko, L. Kalvans, and M. Tamanis, Nonlinear magneto-optical resonances for systems with $J \sim 100$ observed in $K_2$ molecules, Phys. Rev. A **85**, 013421 (2012).

[32] A. Savitzky and M. J. E. Golay, Smoothing and differentiation of data by simplified least squares procedures, Anal. Chem. **36**, 1627 (1964).

[33] A. Sargsyan, G. Hakhumyan, C. Leroy, Y. Pashayan-Leroy, A. Papoyan, D. Sarkisyan, and M. Auzinsh, Hyperfine Paschen-Back regime in alkali metal atoms: Consistency of two theoretical considerations and experiment, J. Opt. Soc. Am. B **31**, 1046 (2014).

[34] D. J. Whiting, E. Bimbard, J. Keaveney, M. A. Zentile, C. S. Adams, and I. G. Hughes, Electromagnetically induced absorption in a nondegenerate three-level ladder system, Opt. Lett. **40**, 4289 (2015).

[35] M. Auzinsh, A. Berzins, R. Ferber, F. Gahbauer, and U. Kalnins, Spatial dynamics of laser-induced fluorescence in an intense laser beam: An experimental and theoretical study with alkali-metal atoms, Phys. Rev. A **93**, 033403 (2016).

[36] J. Alnis, K. Blushs, M. Auzinsh, S. Kennedy, N. Shafer-Ray, and E. R. I. Abraham, The Hanle effect and level crossing spectroscopy in Rb vapour under strong laser excitation, J. Phys. B: At., Mol. Opt. Phys. **36**, 1161 (2003).

[37] A. B. Matsko, O. Kocharovskaya, Y. Rostovtsev, G. R. Welch, A. S. Zibrov, and M. O. Scully, Slow, ultraslow, stored and frozen light, in *Advances in Atomic, Molecular, and Optical Physics*, Vol. 46, edited by B. Bederson (Academic Press, New York, 2001), pp. 191–242.

[38] K. Bergmann, H.-C. Nägerl, C. Panda, G. Gabrielse, E. Miloglyadov, M. Quack, G. Seyfang, G. Wichmann, S. Ospelkaus, A. Kuhn, S. Longhi, A. Szameit, P. Pirro, B. Hillebrands, X.-F. Zhu, J. Zhu, M. Drewsen, W. K. Hensinger, S. Weidt, T. Halfmann, H.-L. Wang, G. S. Paraoanu, N. V. Vitanov, J. Mompart, T. Busch, T. J. Barnum, D. D. Grimes, R. W. Field, M. G. Raizen, E. Narevicius, M. Auzinsh, D. Budker, A. Pálffy, and C. H. Keitel, Roadmap on STIRAP applications, J. Phys. B: At., Mol. Opt. Phys. **52**, 202001 (2019).

[39] P. W. Milonni, *Fast Light, Slow Light, and Left-Handed Light* (Institute of Physics, Bristol, 2005).

[40] E. Arimondo, Coherent population trapping in laser spectroscopy, Prog. Opt. **35**, 257 (1996).

[41] O. Kocharovskaya, Amplification and lasing without inversion, Phys. Rep. **219**, 175 (1992).

[42] S. M. Rochester and D. Budker, Atomic polarization visualized, Am. J. Phys. **69**, 450 (2001).

[43] I. Khriplovich and S. Lamoreaux, *CP Violation without Strangeness: Electric Dipole Moments of Particles, Atoms, and Molecules*, Theoretical and Mathematical Physics (Springer, Berlin, 1997).

[44] W. B. Cairncross and J. Ye, Atoms and molecules in the search for time-reversal symmetry violation, Nat. Rev. Phys. **1**, 510 (2019).